# Electronic Supplementary Information

## Amorphous $SiO_2$-based All-Inorganic Self-Supporting Nanofiber Membrane: A Flexible and Breathable Sensing Platform for $NO_2$ Detection

Jia Liu,[a‡] Qian Yu,[a‡] Yumeng Liu,[a] Xinlei Zhang,[a] Zhibo Yang,[b] Xiaoqiang Yin,[b] Hongbing Lu,[a,*] Jinniu Zhang,[c,*] Jianzhi Gao[a,*] and Benpeng Zhu[d,*]

[a] School of Physics and Information Technology, Shaanxi Normal University, Xi'an 710062, China. E-mail: hblu@snnu.edu.cn; jianzhigao@snnu.edu.cn

[b] Shenzhen BYD Lithium Battery Company Limited, Shenzhen, 518000, China

[c] School of Science, Xi'an University of Posts and Telecommunications, Xi'an 710121, China. E-mail: jinniuzhang@xupt.edu.cn

[d] School of Optical and Electronic Information, Wuhan National Laboratory for Optoelectronics, Huazhong University of Science and Technology, Wuhan 430074, China. E-mail: benpengzhu@hust.edu.cn

† Electronic supplementary information (ESI) available. See DOI:

‡ These authors contributed equally.

**Preparation of FSS NF sensors with different Pd contents.**

Other FSS NF sensors with varied PdO contents were prepared by adding 0.5 mg, 4 mg, and 8 mg of $PdCl_2$ to Sn sols, respectively. The remaining manufacturing steps were identical to those of the FSS PdO–$SnO_2$–$SiO_2$/$SiO_2$ sensor. The corresponding sensors were labeled as (0.5 mg) PdO–$SnO_2$–$SiO_2$/$SiO_2$ NF sensor, (4 mg) PdO–$SnO_2$–$SiO_2$/$SiO_2$ NF sensor, and (8 mg) PdO–$SnO_2$–$SiO_2$/$SiO_2$ NF sensor, respectively.

**Fabrication of commercially available PET sensors**

Briefly, PdO-$SnO_2$ NFs was mixed with 70 ethanol to obtain the corresponding slurry. The slurry was then dripped on a commercially available sensor substrate made of PET, with a spacing of almost 0.1 mm, in order to obtain the commercially available PET sensor. All the fabricated sensors were aged in air at 80 °C for 2 h.

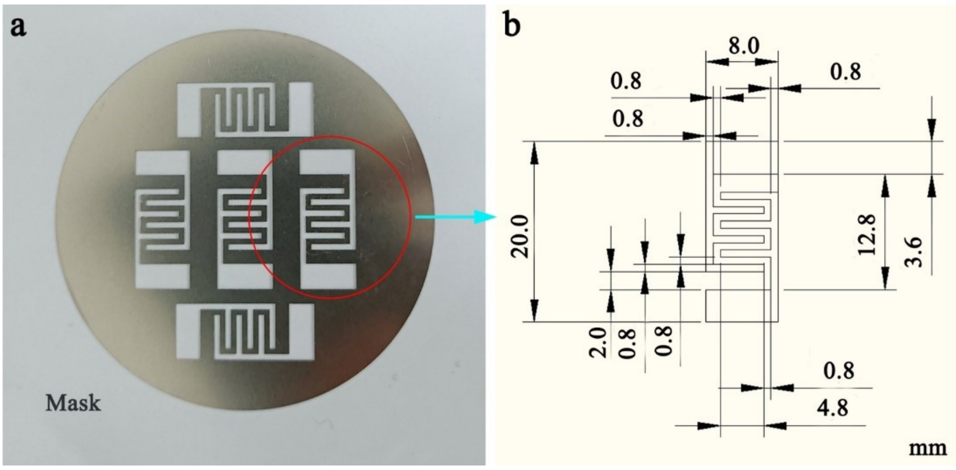


**Fig. S1** Photograph of the electrode mask and its detailed structure.

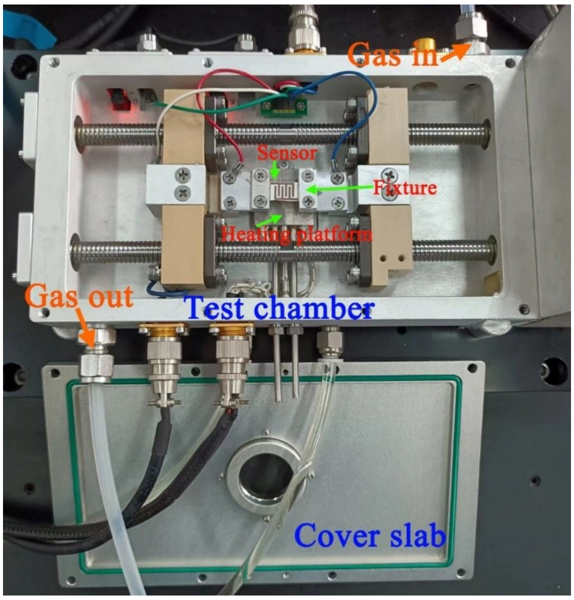


**Fig. S2** The sensing testing chamber of AES-4SD flexible gas sensing analysis system.

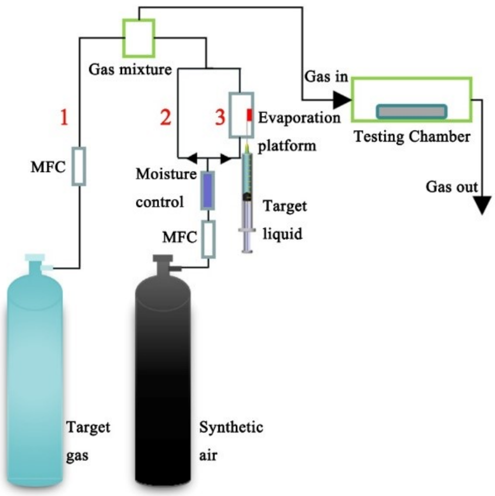


**Fig. S3** The flow chart of the dynamic gas and liquid distribution system.

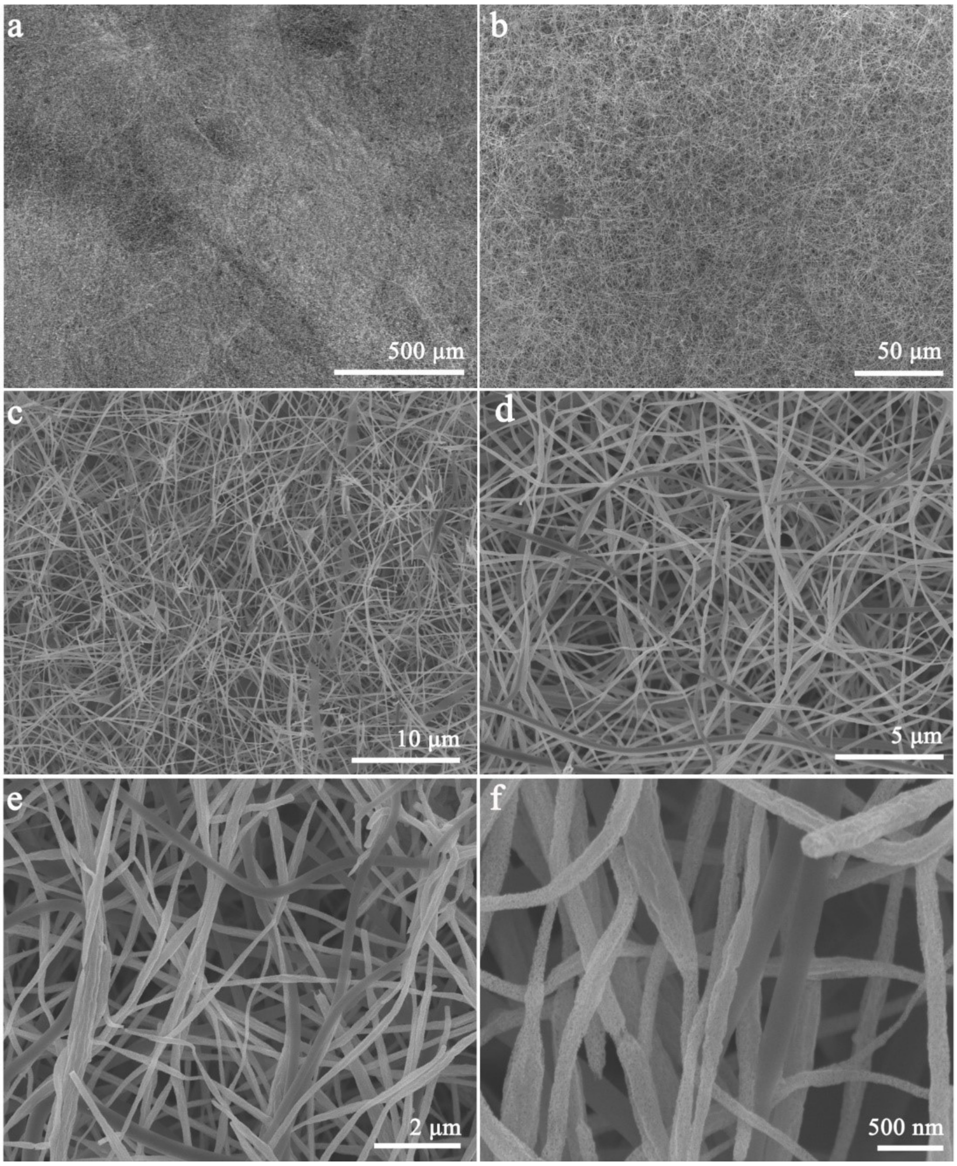


**Fig. S4** SEM images with different magnifications of PdO–$SiO_2$–$SnO_2$/$SiO_2$ NF membrane.

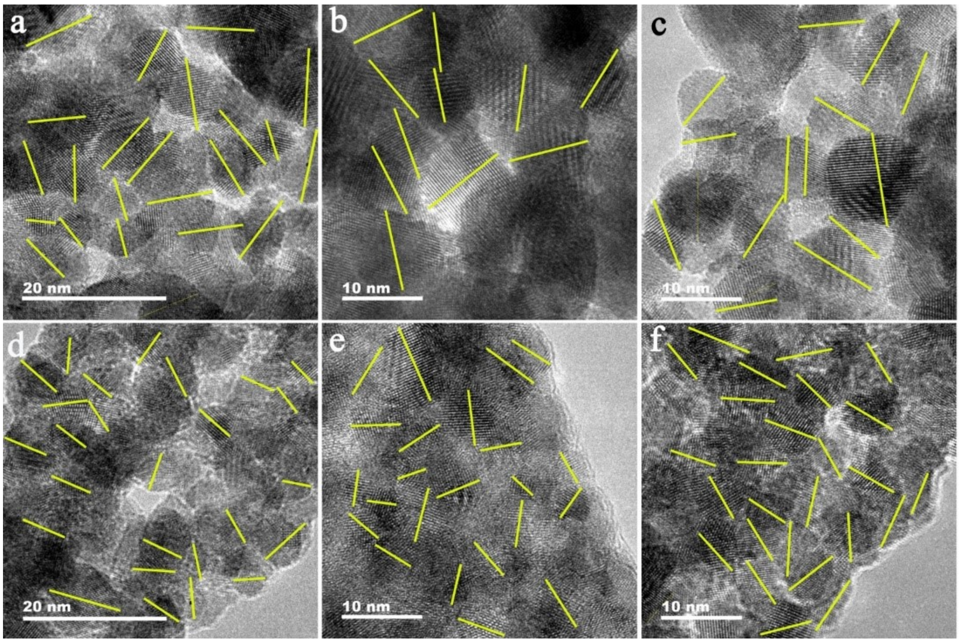


**Fig. S5** HRTEM images of (a–c) $SnO_2$ NF from $SnO_2$–$SiO_2$/$SiO_2$ NFs. (d–f) PdO–$SnO_2$ NF from PdO–$SnO_2$–$SiO_2$/$SiO_2$ NFs.

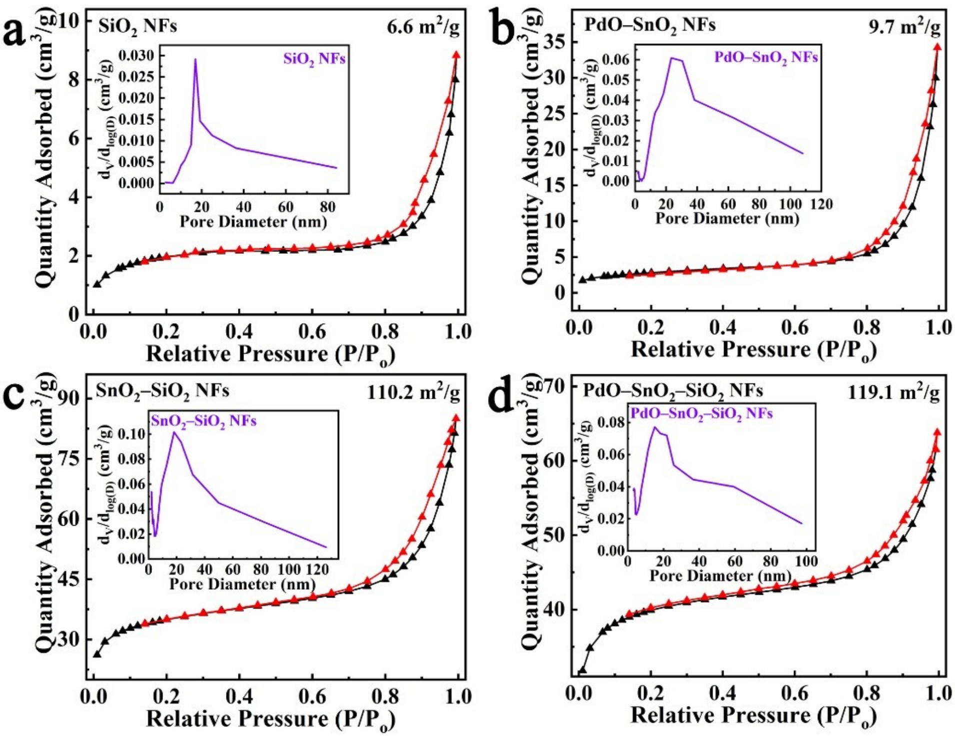


**Fig. S6** $N_2$ adsorption–desorption isotherms of (a) $SiO_2$, (b) PdO–$SnO_2$, (c) $SnO_2$–$SiO_2$, and (d) PdO–$SnO_2$–$SiO_2$ NFs. The insets are the corresponding pore size distribution curves.

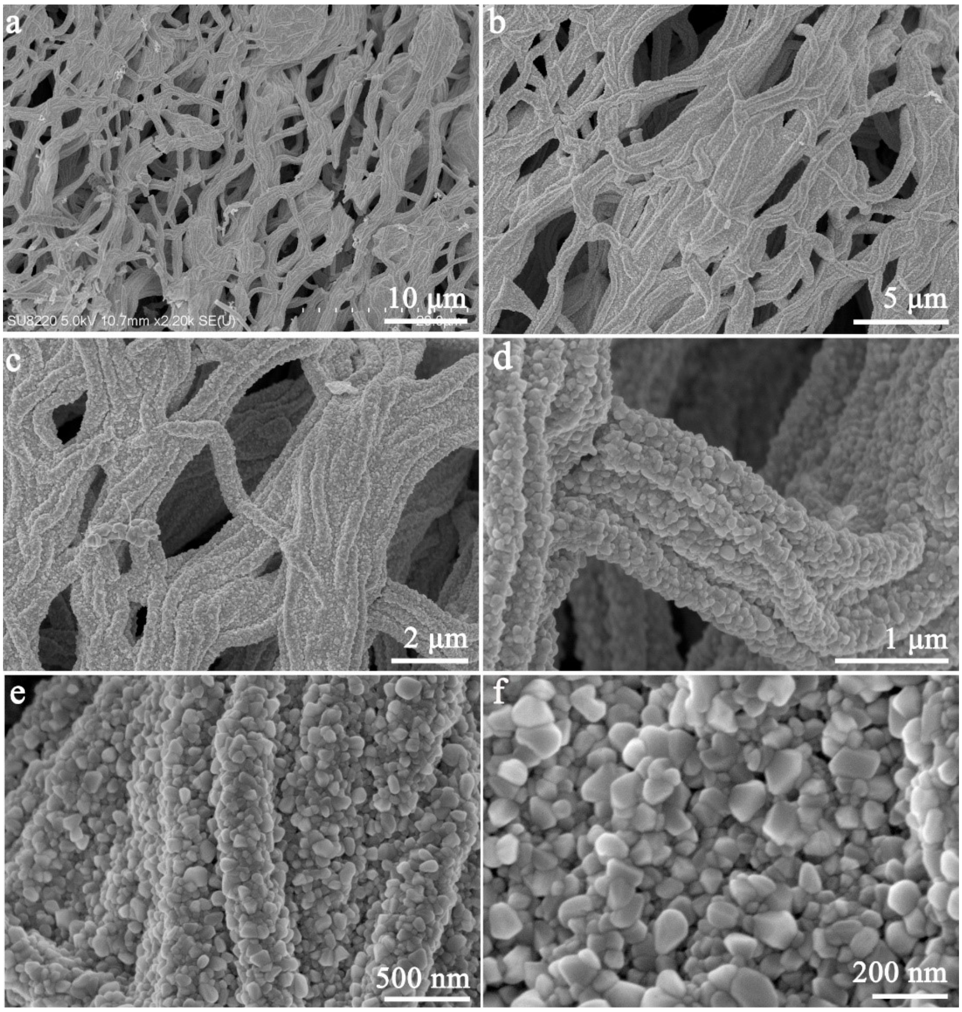


**Fig. S7** SEM images with different magnifications of PdO–$SnO_2$ NFs.

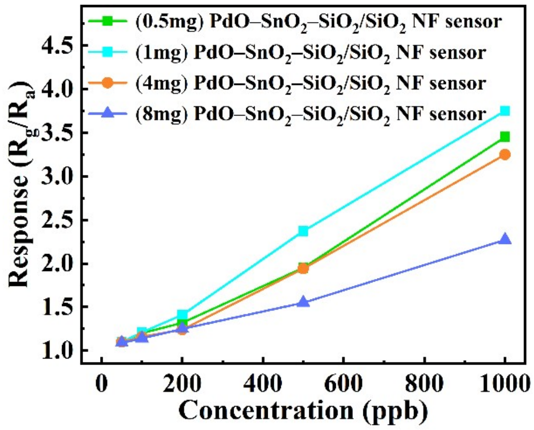


**Fig. S8** Responses of the sensors with various PdO contents to various concentrations of $NO_2$ at room temperature.

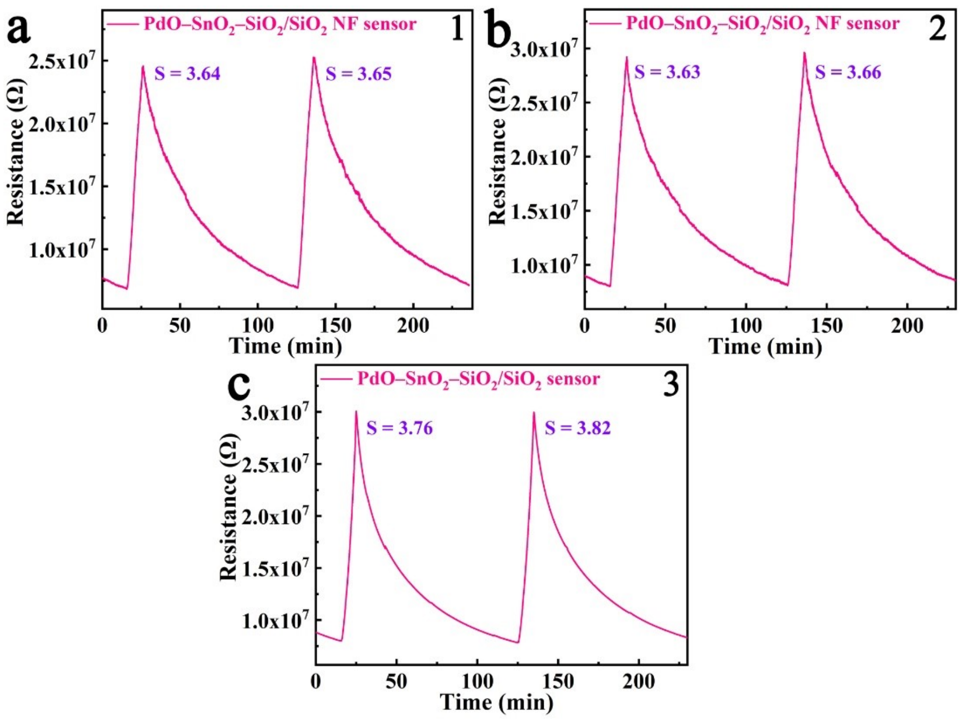


**Fig. S9** Resistance–time curves of the other 3 batches of FSS PdO–$SnO_2$–$SiO_2$/$SiO_2$ NF sensors to 1000 ppb $NO_2$ at RT.

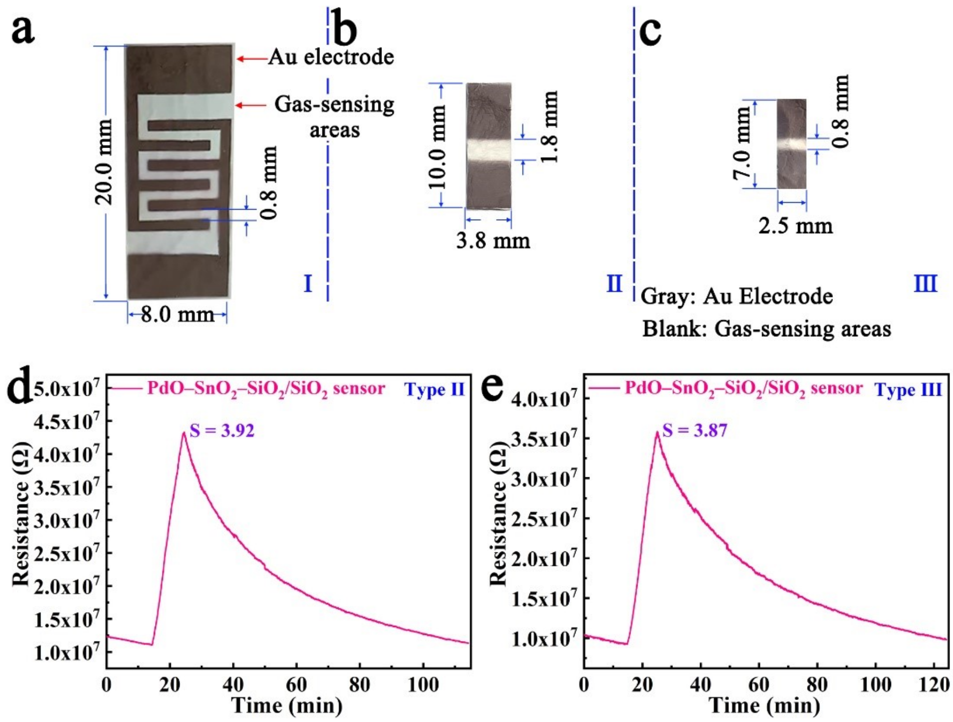


**Fig. S10** Photographs of FSS PdO–$SnO_2$–$SiO_2$/$SiO_2$ NF sensors with different sizes: (a) type I used in this work, (b) type II, and (c) type III. Resistance–time curves of the FSS PdO–$SnO_2$–$SiO_2$/$SiO_2$ NF sensors to 1000 ppb $NO_2$ at RT with different sizes: (d) type II and (e) type III.

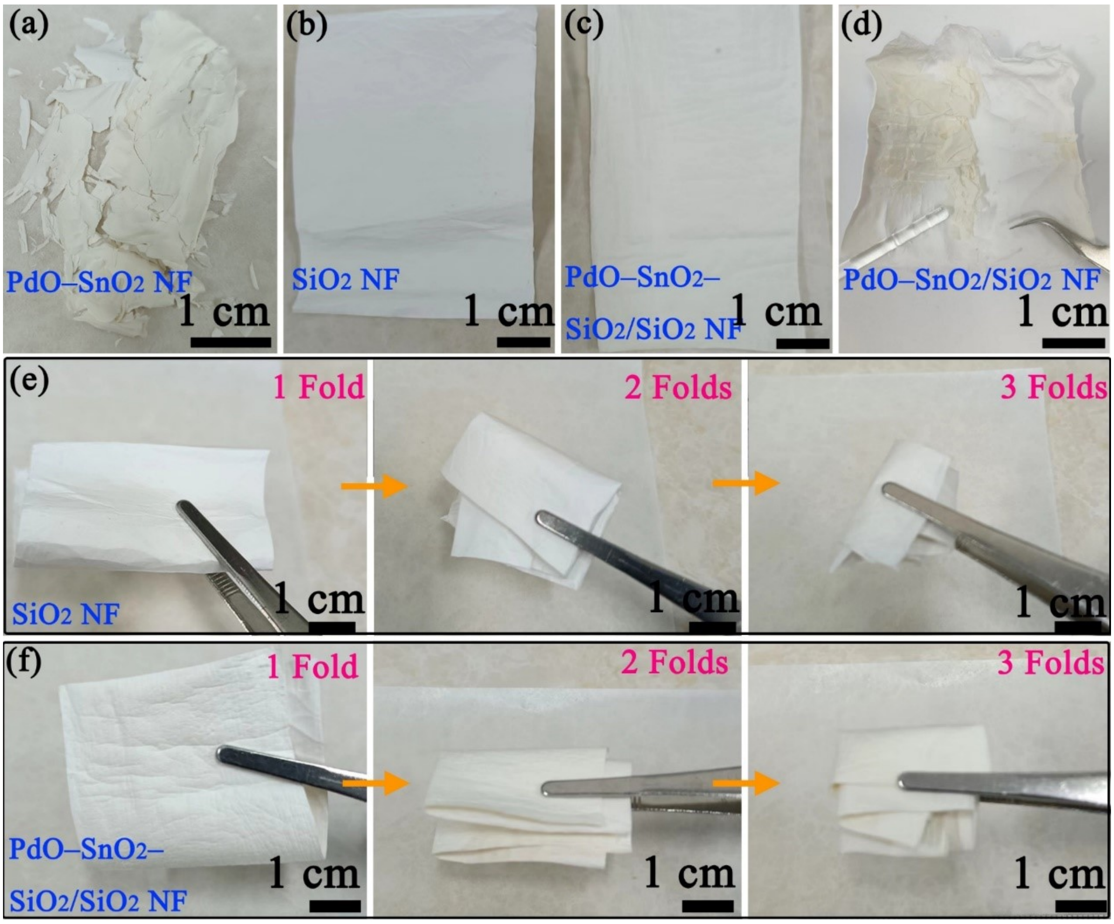


**Fig. S11** Photographs of (a) PdO–$SnO_2$ NF membrane, (b) $SiO_2$ NF membrane, (c) PdO–$SnO_2$–$SiO_2$/$SiO_2$ NF and (d) PdO–$SnO_2$/$SiO_2$ NF membranes. Folded photographs of (e) $SnO_2$ NF membrane and (f) PdO–$SnO_2$–$SiO_2$/$SiO_2$ NF membranes.

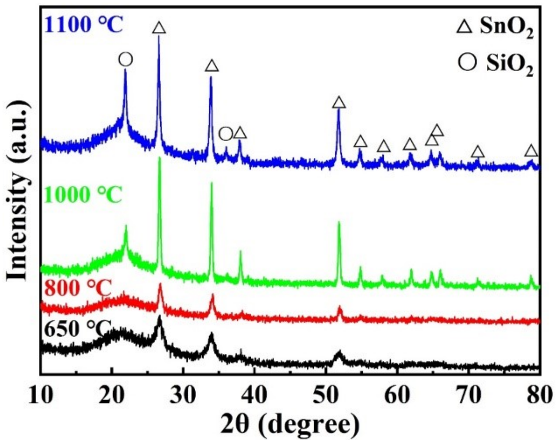


**Fig. S12** XRD patterns of PdO–$SnO_2$–$SiO_2$/$SiO_2$ NF membrane at different calcination temperatures.

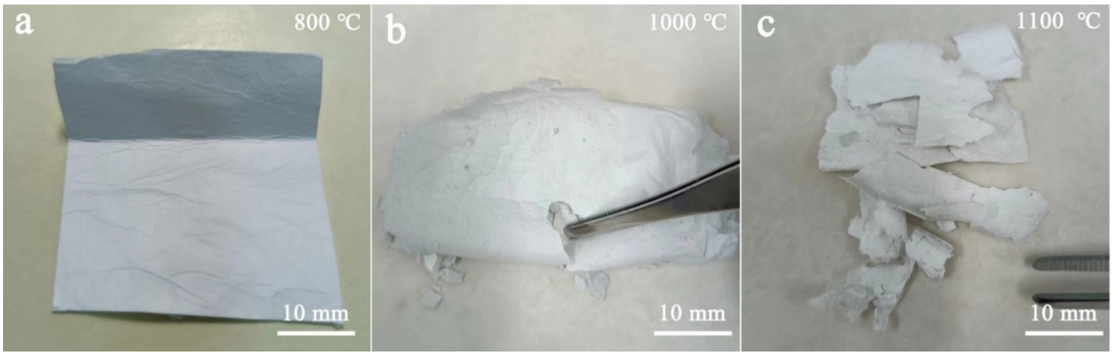


**Fig. S13** Photographs of PdO–$SnO_2$–$SiO_2$/$SiO_2$ NF membrane at different calcination temperatures: (a)800 °C, (b)1000 °C, and (c) 1100 °C.

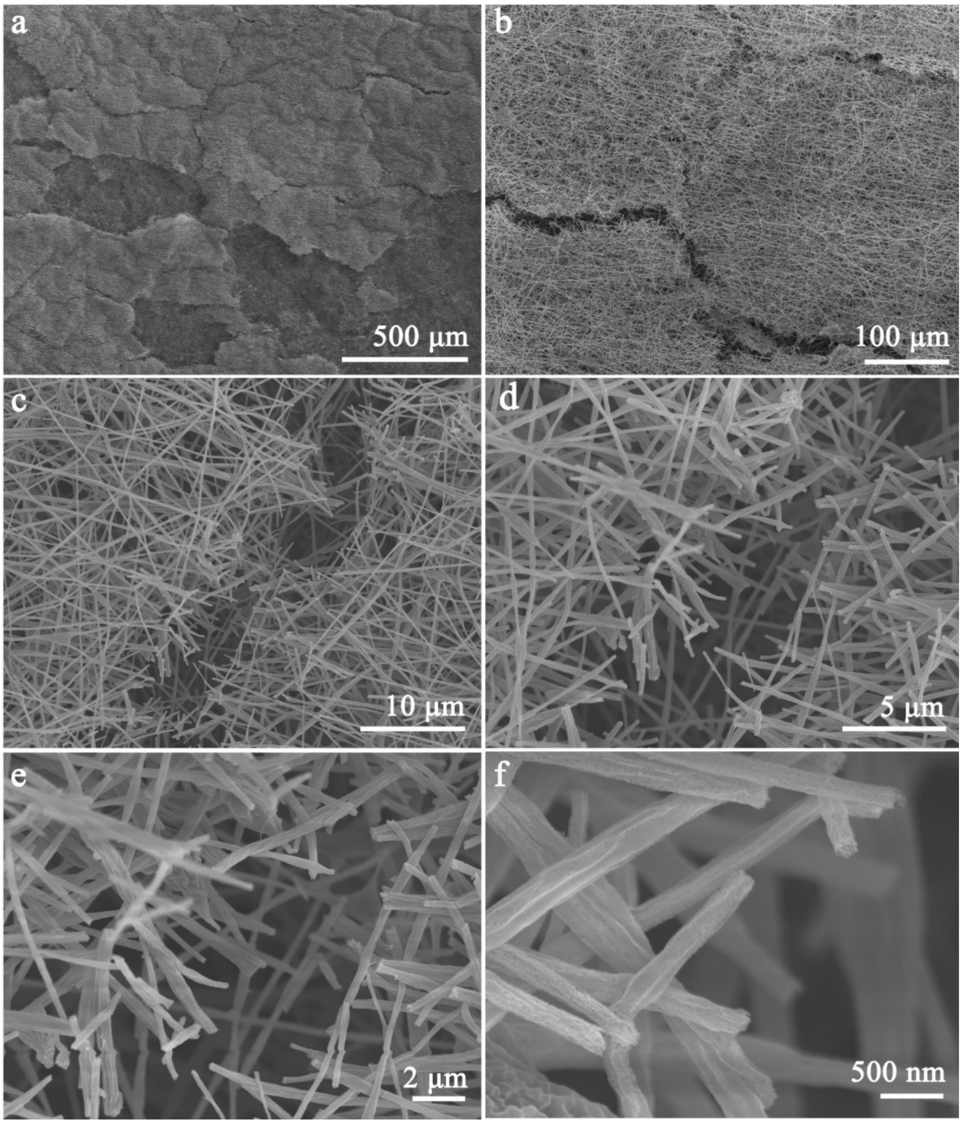


**Fig. S14** SEM images with different magnifications of PdO–$SnO_2$/$SiO_2$ NF membrane.

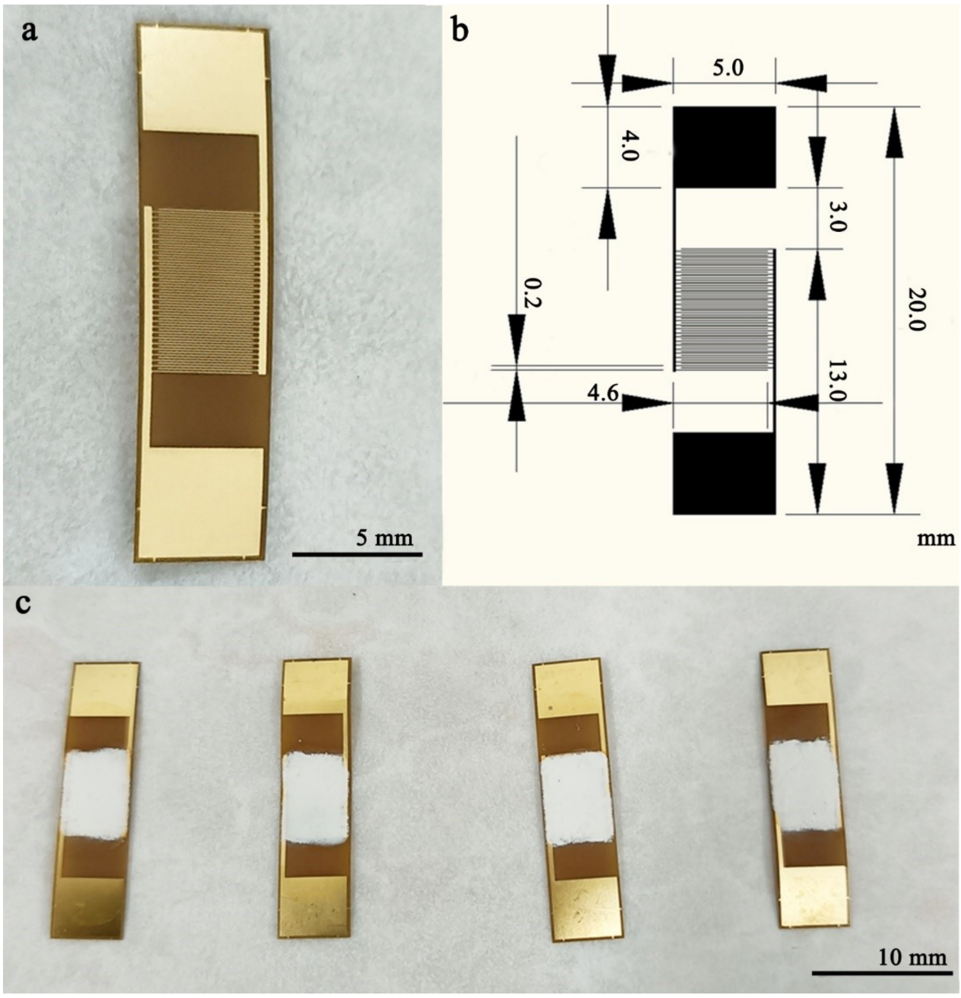


**Fig. S15** (a,b) Photographs of the commercially available sensor substrate and the detailed structure. (c) Photographs of commercial PET-based PdO–$SnO_2$ NF sensors.

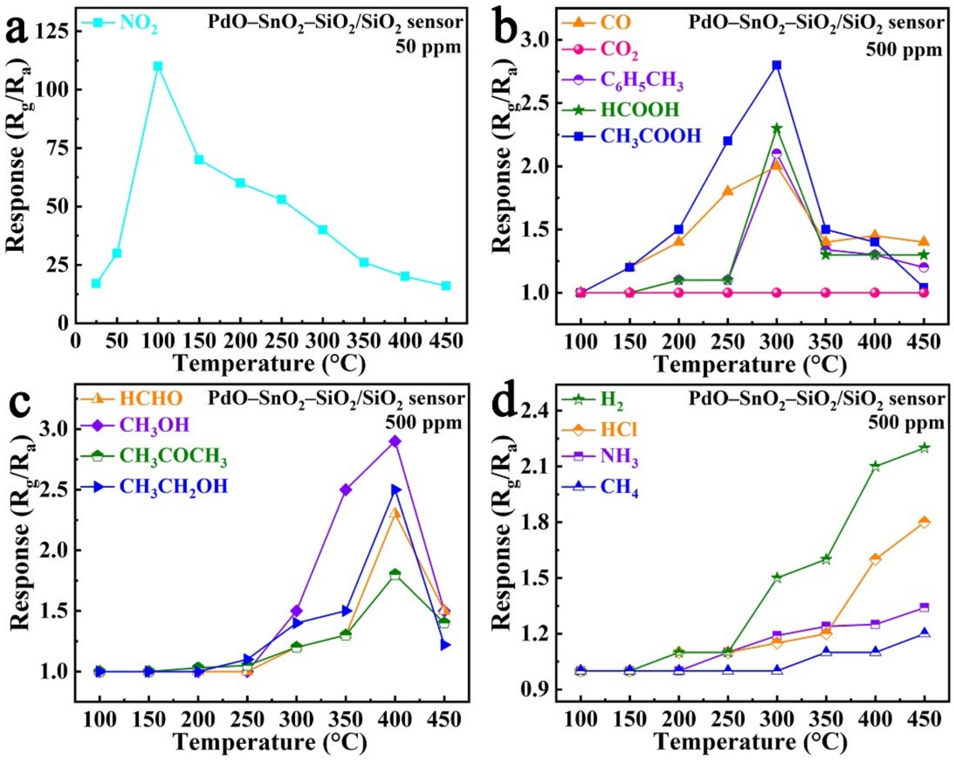


**Fig. S16** Response–temperature curves of the FSS PdO–$SnO_2$–$SiO_2$/$SiO_2$ NF sensor to various gases.

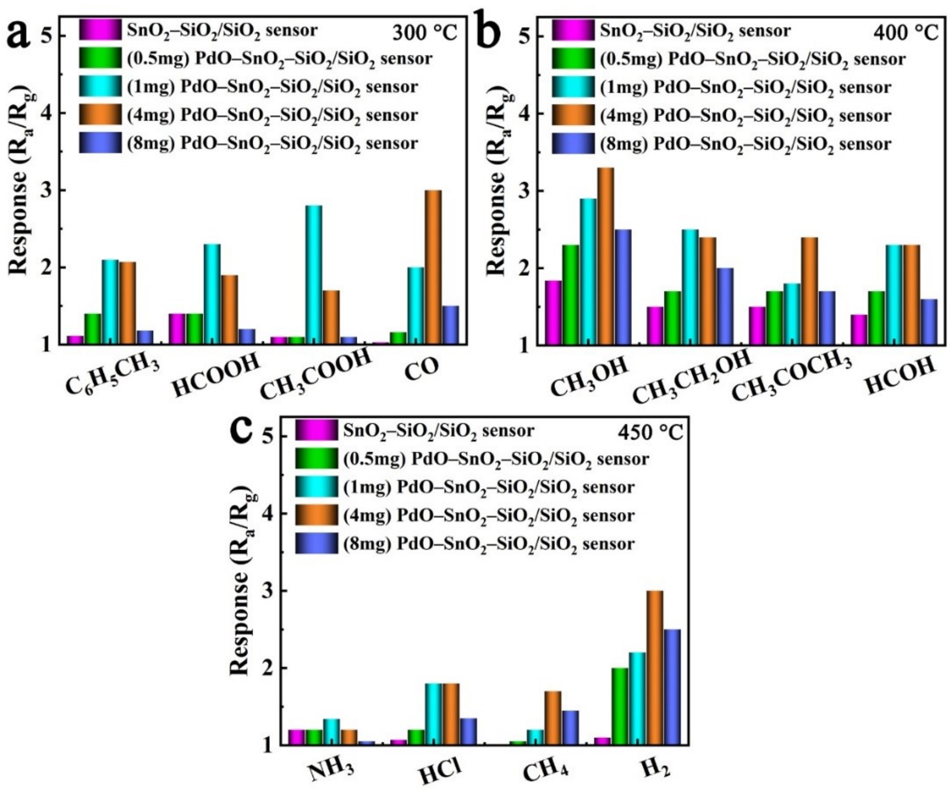


**Fig. S17** Histograms of the responses of the sensors with various PdO contents to various gases at different temperatures: (a) 300 °C, (b) 400 °C, and (c) 450 °C.

**Table S1** Adsorption energy and Bader charge transfer of $SnO_2$, Pd–$SnO_2$, and Pt–$SnO_2$ toward various gas molecules in reported literatures.

| | Gas molecules | Adsorption energy (eV) | Bader charge transfer ($e^-$) |
|---|---|---|---|
| $SnO_2$ | $NO_2$ | -0.9,[1] -089[2] | 0.58[1] |
| | CO | -0.49[3] | 0 ~ 0.14[3] |
| | $C_6H_5CH_3$ | -0.10,[4] -0.28[2] | 0.22[2] |
| | HCHO | 0.04,[1] -0.26[2] | 0.01,[1] 0.17[2] |
| | $CH_3COCH_3$ | 0.41,[4] -0.22[2] | 0.06[2] |
| | $CH_3OH$ | 0.19[4] | / |
| | $CH_3CH_2OH$ | -0.03,[1] 0.72[4] | 0.003[1] |
| | $H_2$ | -0.26,[5] -0.12 ~ -0.29[6] | 0.004[5] |
| | $NH_3$ | -0.19[4] | 0.12[1] |
| | $CH_4$ | -0.03[1] | 0.01[1] |
| Pd–$SnO_2$ | $NO_2$ | -1.24[2] | / |
| | CO | -0.63[7] | 0.13[7] |
| | $CH_4$ | -0.47[8] | 0.10[8] |
| Pt–$SnO_2$ | $NO_2$ | -1.73[2] | 0.39[2] |
| | $C_6H_5CH_3$ | -0.43[2] | 0.22[2] |
| | HCHO | -0.52[2] | 0.17[2] |
| | $CH_3COCH_3$ | -0.30[2] | 0.06[2] |

**References**


1. Y. Zhang, Y. Jiang, Z. Yuan, B. Liu, Q. Zhao, Q. Huang, Z. Li, W. Zeng, Z. Duan and H. Tai, *Small*, 2023, **19**, 2303631.
2. Z. Song, W. Tang, Z. Chen, Z. a. Wan, C. L. J. Chan, C. Wang, W. Ye and Z. Fan, *Small*, 2022, **18**, 2203212.
3. M. Eslamian, A. Salehi and E. Nadimi, *Surface Science*, 2021, **708**, 121817.
4. L. Zhang, J. Shi, Y. Huang, H. Xu, K. Xu, P. K. Chu and F. Ma, *ACS applied materials & interfaces*, 2019, **11**, 12958-12967.
5. W. Du, W. Si, W. Du, T. Ouyang, F. Wang, M. Gao, L. Wu, J. Liu, Z. Qian and W. Liu, *Journal of Alloys and Compounds*, 2020, **834**, 155209.
6. A. Umar, H. Y. Ammar, R. Kumar, T. Almas, A. A. Ibrahim, M. S. AlAssiri, M. Abaker and S. Baskoutas, *International Journal of Hydrogen Energy*, 2020, **45**, 26388-26401.
7. P. Bechthold, M. E. Pronsato and C. Pistonesi, *Applied Surface Science*, 2015, **347**, 291-298.
8. L. Xue, Y. Ren, Y. Li, W. Xie, K. Chen, Y. Zou, L. Wu and Y. Deng, *Small*, 2023, **19**, 2302327